Heliyon

ELSEVIER

Check for
updates

Effects of transition metals incorporated into perovskite crystals on the electronic structures and magnetic properties by first-principles calculation

Atsushi Suzuki[*], **Takeo Oku**

Department of Materials Science, School of Engineering, The University of Shiga Prefecture, 2500 Hassaka, Hikone, Shiga, 522-8533, Japan

[*] Corresponding author.

E-mail address: suzuki@mat.usp.ac.jp (A. Suzuki).

Abstract

Additive effects of transition metals ($M = Cr^{2+}$, Co^{2+}, Cu^{2+} and Y^{3+}) on the electronic structures and magnetic properties of formamidinium lead halide perovskite compounds ($FAPbI_3$, where $FA = NH_2CHNH_2^+$) were investigated by first-principle calculation using density functional theory. In the case of Cr^{2+}, Cu^{2+} and Y^{3+}-incorporated $FAPbI_3$ perovskite crystals, the electron density distribution of *d-p* hybrid orbital on the transition metal and iodine halogen-atoms were delocalized at frontier orbital. The total and partial density of state appeared the $3d$-*p* hybrid orbital near the frontier orbital with narrowing band gap, yielding the wide broad absorption in the near-infrared region. The electronic correlation worked in between the localized spin on $3d$ orbital of the metal, and the itinerant carriers on the $5p$ orbital of the iodine halogen ligand and the $6p$ orbital of the lead atom in the perovskite crystal. The vibration behavior of the Raman and Infrared spectra were associated with change of polarization and slight distortion near the coordination structure. The considerable splitting of chemical shift of [127]I-NMR and [207]Pb-NMR in the Co^{2+}

and Cu^{2+}-incorporated $FAPbI_3$ crystals were caused by crystal field splitting as Jahn-Teller effect with nearest-neighbor nuclear quadrupole interaction based on the charge distribution.

Keyword: Theoretical chemistry

1. Introduction

Inorganic-organic hybrid perovskite solar cells using mixed-cation and halogen lead hybrid perovskite compounds varied with molar ratio have high potential for applying practical use of photovoltaic device and optical properties. Control of the perovskite crystal structure and the chemical composition ratio using organic cations from methylammonium (MA = $CH_3NH_3^+$), formamidinium [FA = $CH_3(NH_2)_2^+$] [1,2], cesium (Cs) [3], guanidinium [4], divalent metals (lead, tin and bismuth) [5] and halogen anions (Cl^-, Br^-, and I^-) [6, 7, 8] is important factor for optimizing with tuning the photovoltaic and optical properties. The effects of halogen using bromide, iodide and chloride halides, amino cations, and hole-transporting layers on photovoltaic and optical properties were examined [4, 9, 10, 11]. The photovoltaic, transporting and optical properties, infrared (IR) and Raman vibration modes of mixed halogen hybrid perovskites were characterized on the basis of the experimental results together with first-principle calculation using the density functional theory (DFT) and time-dependent (TD)-DFT [12, 13, 14, 15, 16]. The photovoltaic and magnetic mechanisms of mixed-cation and halogen lead hybrid perovskite crystals were clarified by magnetic and spectroscopic techniques using multinuclear (^{14}N, ^{207}Pb, and ^{127}I) magnetic resonance (NMR) spectra [17, 18, 19]. The solid-state NMR spectra and Raman spectra made clear the spin dynamics of formamidinium (FA) and methylammonium (MA) in the perovskite crystal and identification of incorporation of potassium, cesium and rubidium [20]. Recently, manganese (Mn)-incorporated $CH_3NH_3PbI_3$ ($MAPbI_3$) perovskite compounds were studied for applying the photovoltaic and spintronic devices [21, 22]. The photo-induced magnetic mechanisms were based on the electronic structure with intermixing hybrization of the localized $3d$ orbital on the transition metal and itinerant carriers on $6p$ orbital of Pb and $5p$ orbital of I atoms as functions of magnetic interaction and the size of the Fermi surface. The slight perturbation of the ligand field of the $3d$ orbital on the transition metal in the perovskite crystal will cause a change of the photo-induced magnetic properties [23]. For instant, the electronic and magnetic properties of cerium manganese oxide ($CeMnO_3$) with the Mn-$3d$ and Ce-$4d$ electrons were investigated as referred by Ref. [24]. The transition metal incorporated $CeMnO_3$ perovskite crystal with a metallic character is advantage as a candidate material for spintronic application and photo-induced magnetic devices. Experimental investigation on the incorporation of transition metals such as iron (Fe), cobalt (Co)

and copper (Cu) on lead (Pb) site of perovskite crystal was performed for optimization with tuning the electronic structure, energies levels, total density of state within the band gap and optical absorption [25, 26, 27]. For example, the photovoltaic and optical properties of the Cu-incorporated perovskite solar cell were discussed on the basis of the electron correlation between the $3d$ orbital localized on the metal and the $5p$ orbital of the halogen atom near the metal-ligand structure in the perovskite crystal. The Cu-based perovskite solar cell had the slight perturbation of coordination structure as Jahn-Teller effect with tuning the crystal field splitting, which influenced the magnetic and optical properties in the ultraviolet and near-infrared (NIR) region [28]. The transition metal-based perovskite solar cells had the high potential to promote the photocurrent generation, transporting and optical properties with a wide range of optical absorption near NIR. Incorporation of the transition metal into the perovskite crystal modified the crystal structure, phase, work function and band gap. Raman and optical spectra of the Co based perovskite solar cell using mixed halides compounds varied with the molar ratio of the transition metal and halogen anions were characterized [29]. Experimental investigations on the photovoltaic properties of methylammonium lead perovskite solar cell with partially replacing lead atom with transition metals such as Co, Cu, Fe, Mg, Mn, Ni, Sn, Sr and Zn were performed [30, 31, 32, 33, 34]. Especially, adjusting the molar ratio of Pb and Co in the mixed-metal perovskite crystal modified the perovskite work function, the photovoltaic performance with the power conversion efficiencies and open-circuit voltages. The transition metal incorporated into the perovskite crystal have the electron correlation between itinerant electron at conduction state and localized spin on $3d$ orbital in the transition metal at the multiplet states. The transition metals of Co, chromium (Cr), Cu and yttrium (Y) have the different extent of intermixing of hybrid orbitals between the central metal and halogen ligand with crystal splitting of the $3d$ and $4d$ orbitals in coordination structure, which influences the carrier generation, mobility, photovoltaic, magnetic and optical properties. Incorporation of the transition metals into the perovskite crystal is important role of optimizing with tuning the electronic structure and electronic correlation related to the photovoltaic and magnetic properties with the optical absorption in ultraviolet-visible-near-infrared region.

The purpose of this work is to investigate additive effect of transition metal on the electronic structure, the optical and magnetic properties of formamidinium lead halide perovskite compounds (FAPbI$_3$, where FA = NH$_2$CHNH$_2^+$). The additive effects of transition metal such as Co, Cr, Cu and Y in the FAPbI$_3$ perovskite crystal on the electronic structures, chemical shifts of [207]Pb-NMR and [127]I-NMR spectra, optical absorption, vibration mode of Raman and IR spectra will be investigated by first-principles calculation using the density functional theory. The photovoltaic and optical properties, and magnetic interaction will be discussed on the basis of the electronic structures including the total and partial density of state (DOS and pDOS),

the electron density distribution, occupancy and energy levels of the *5p* orbital of the iodine halogen atom, the *3d* and *4d* orbitals of Co^{2+}, Cr^{2+}, Cu^{2+}, Y^{3+} and the *6p* orbital of the Pb atom near frontier orbital.

2. Calculation

The electronic structures of the perovskite crystal were single-point calculated using experimental parameters based from X-ray diffraction patterns combined with *ab initio* quantum calculation based on the unrestricted Hartree-Fock (HF) method, the hybrid functional theory (DFT) and the Perdew−Burke−Ernzerhof (PBE)-based hybrid functional (PBEPBE) using unrestricted B3LYP (UB3LYP) with LANL2MB as the basis set (Gaussian 09). The perovskite crystals with *d* transition metal have strong electron correlation. The special treatment on the quantum calculation was performed by approximation. In general, local density approximation (LDA) corresponds to uniform electron density distribution. The no-uniformity of the electron in *d*-orbital of the transition metal needs to be considered. The electron exchange-correlation is associated with inhomogeneous distribution of electron density in *d*-orbital of the transition metal in ligand structure. The electron correlation influences the electronic structure, the metal-ligand interaction and the anisotropic parameter of the magnetic properties. The generalized gradient approximation (GGA) and hybrid GGA takes into account the electron correlation based on the gradient of the electron density. For *3d* transition metal in the ligand structure, the calculation accuracy of hybrid density functional theory (DFT) using B3LYP and the Perdew−Burke−Ernzerhof (PBE)-based hybrid functional (PBEPBE) is higher than that of LDA. Using LDA, the band gap is underestimated. The hybrid DFT, PBEPBE and the Heyd−Scuseria−Ernzerhof hybrid functional (HSE) can calculate the electronic structures with high precision. For the metal incorporated perovskite crystal with supercells of $2 \times 2 \times 2$ as cluster model and the $FAPbI_3$ perovskite crystal as cluster model and periodic structure with cell range of 100, we employed the quantum calculation using hybrid DFT and PBEPBE using UB3LYP with LANL2MB as the basis set. The perovskite compounds form in a cubic crystal phase with a lattice constant of 6.36 Å [29, 32, 33, 34, 35]. As the isolated dilution system, part of the Pb atom at the B-site was substituted with the transition metal atom for one-atom substitution at the center of the cubic structure. The metal-incorporated $FAPbI_3$ cubic structures as cluster model with supercells of $2 \times 2 \times 2$ were fixed to be +8 as the positive charge. As reference, the $FAPbI_3$ perovskite crystal with supercells of $2 \times 2 \times 2$ as cluster model were fixed at +8 as positive charge. In the case of the periodic structure at neutral state, cell range and number of *k* point were designated to be 100 and 10 as condition. In the case of the element-substitution system, cluster model based on the experimental crystal structure was used for the quantum calculation. The structures had the slight deformation with

the local strain near the ligand field. The crystal and thermodynamic stability is depending on periodicity, supercell and the perovskite crystal size. The experimental structure of reference was used as the initial structure [34, 35]. Optimization of the cluster model while maintaining the crystal symmetry was not performed to cause broking the cubic structure. The single-point energy calculation of the cluster model with supercells of $2 \times 2 \times 2$ and positive charge of +8 was performed as not to disturb the cubic structure, similarly to the standard case using the $FAPbI_3$ perovskite crystal based on the experimental results.

The numbers of quantum spins in the metal (M)-incorporated $FAPbI_3$ and $FAPbI_3$ crystals are assumed to be quintet (S = 4) state at M = Cr^{2+}, quartet (S = 3/2) state at M = Co^{2+}, doublet (S = 1/2) states at M = Cu^{2+} and Y^{3+}, and singlet (S = 0) state at M = Pb^{2+}, respectively. As the isolated dilution system, the mole ratio of the transition metal to Pb metal was adjusted to be 1:26. The concentration of the metal atom was maintained at less than 5% so as not to generate symmetry breaking of the crystal with suppression of strong exchange interactions in the perovskite crystal. The effect of the ionic radius is assumed to be weak in an isolated dilution system. The magnetic dilution system did not exist the magnetic orientation based on the strong exchange interaction. The paramagnetic calculations of the paramagnetic atom incorporated perovskite crystal as the magnetic dilution system were performed for making clear the magnetic parameters without strong exchange interaction. The ferromagnetic and antiferromagnetic calculations were not performed.

The total and partial DOS (TDOS and pDOS), the occupancy of the 3*d* orbital on the transition metal, 6*s*, the 5*p* and 6*p* orbitals of the I and Pb atoms around highest occupied molecular orbital (HOMO), and lowest unoccupied molecular orbital (LUMO), and the HOMO-LUMO band gap (E_g) were calculated. As standard reference, the electronic structure of the $FAPbI_3$ perovskite cubic structure with supercells of $2 \times 2 \times 2$ at charge of +8 and periodic structure with cell range of 100 at neutral state was calculated by *ab initio* quantum calculation based on the DFT using UB3LYP and PBEPBE with LANL2MB as the basis set (Gaussian 09). Comparison between the calculation and experimental results was performed. The Mulliken atomic charges, electron and spin density distributions, and electrostatic potential (ESP) in the perovskite crystals were estimated by Mulliken population analysis. The optical absorption spectra, the excited energy, wavelength and oscillator strength were calculated by time-dependent DFT (TD-DFT) using UB3LYP with LANL2MB as the basis set. The vibration modes in Raman and IR spectra were calculated by DFT using frequency mode. From the vibration calculation, the structure had real and imaginary vibration, which was judged to be higher-order saddle point. The isotropic chemical shifts of [127]I-NMR and [207]Pb-NMR were calculated by DFT using NMR and gauge-including atomic orbitals (GIAO) with UB3LYP and LANL2MB as the basis set. The calculation conditions were applied to short-range interactions. The long-range interactions based on the periodicity of the

metal-incorporated FAPbI$_3$ perovskite crystal will not be taken into consideration. The photovoltaic and optical properties, and magnetic interactions will be discussed by the electronic structure with the electronic correlation of coordination structure near ligand field and the nuclear magnetic interaction in the perovskite crystal.
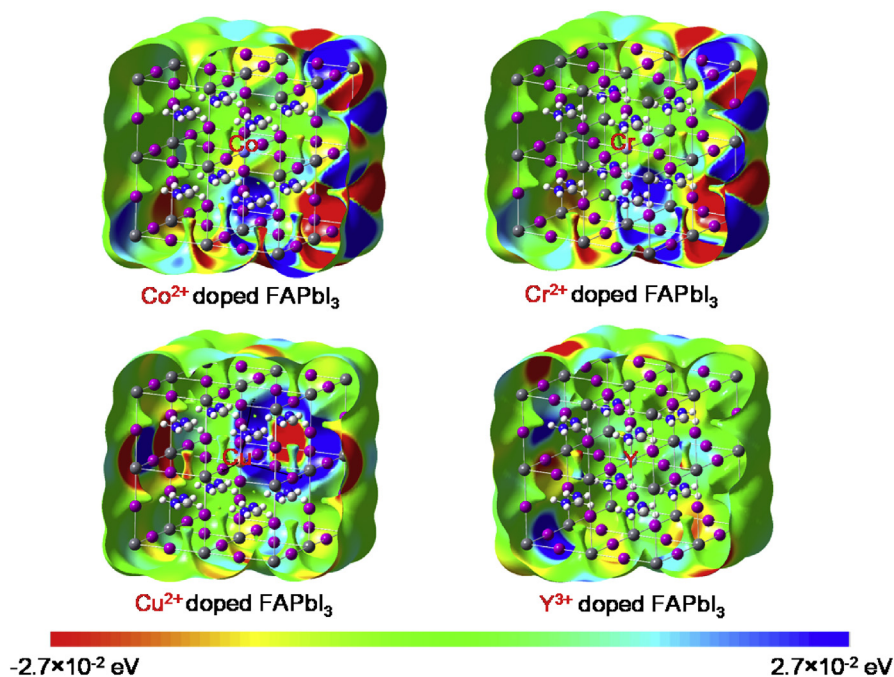
3. Results and discussion

The electronic structures at HOMO and LUMO of the metal (M)-incorporated FAPbI$_3$ perovskite crystals are shown in Fig. 1. As shown in Fig. 1, single metal atom (M = Co^{2+}, Cr^{2+}, Cu^{2+} and Y^{3+}) was incorporated into a FAPbI$_3$ perovskite crystal with the cubic structure as the $2 \times 2 \times 2$ supercell. In the case of the Co and Cr-incorporated FAPbI$_3$ perovskite crystals, the electron density distribution on the 5p orbital of the I atom was localized at HOMO. The phases between green and red 5p orbitals on the I atom were inverted. The 5p orbital on the I atom will work function in the charge transfer as the electron-donating orbital at the valence band state. In the case of the Co-incorporated FAPbI$_3$ perovskite crystal, the electron density distribution of the 6p orbital of the Pb atom was localized at LUMO. In the case of the Cr-incorporated FAPbI$_3$ perovskite crystal, the 3d orbital of Cr atom conjugated with the 5p orbital of I atom as ligand was localized at LUMO. The 6p orbital of the Pb atom was slightly existed. In the case of the Cu and Y-incorporated FAPbI$_3$ perovskite crystals, the electron density distribution at HOMO was delocalized on the 3d-p hybrid orbital of the Cu, Y and I atoms. The electron density distribution on the 6p orbital of the Pb atom was localized at LUMO. The orbitals work function in the charge transfer as the electron-accepting orbital at the conducting band state. The optical and magnetic properties depend on the contribution of the coordination structure with electronic correlation between itinerant carriers on the 6p orbital of the Pb atom, the 5p orbital of the I atom and the localized spin on 3d orbital in the Cu and Y atoms as the isolated dilution system.

Electrostatic potential images of the metal (M = Co^{2+}, Cr^{2+}, Cu^{2+} and Y^{3+}) incorporated FAPbI$_3$ perovskite crystals are shown in Fig. 2. The charge distribution on iodine halogen atoms were appeared by slight incorporation of the Co and Cr atoms into the FAPbI$_3$ perovskite crystal. In the case of the Cu^{2+}-incorporated FAPbI$_3$ perovskite crystals, the polarization near the FA cation atom was obtained. In the case of the Y^{3+}-incorporated FAPbI$_3$ perovskite crystal, a small amount of negative charge distribution at iodine halogen atoms were slightly existed by a slight large amount of the positive charge of the Y atom, compared with other cases as listed in Table 1. The charge distribution in the metal-incorporated perovskite crystal will promote to cause the photo-induced charge separation and generation, transporting and magnetic interaction in the correlated system. The magnetic properties of the metal-incorporated perovskite crystal will be associated with the magnetic interaction of nuclear quadrupole interaction based on the charge distribution.
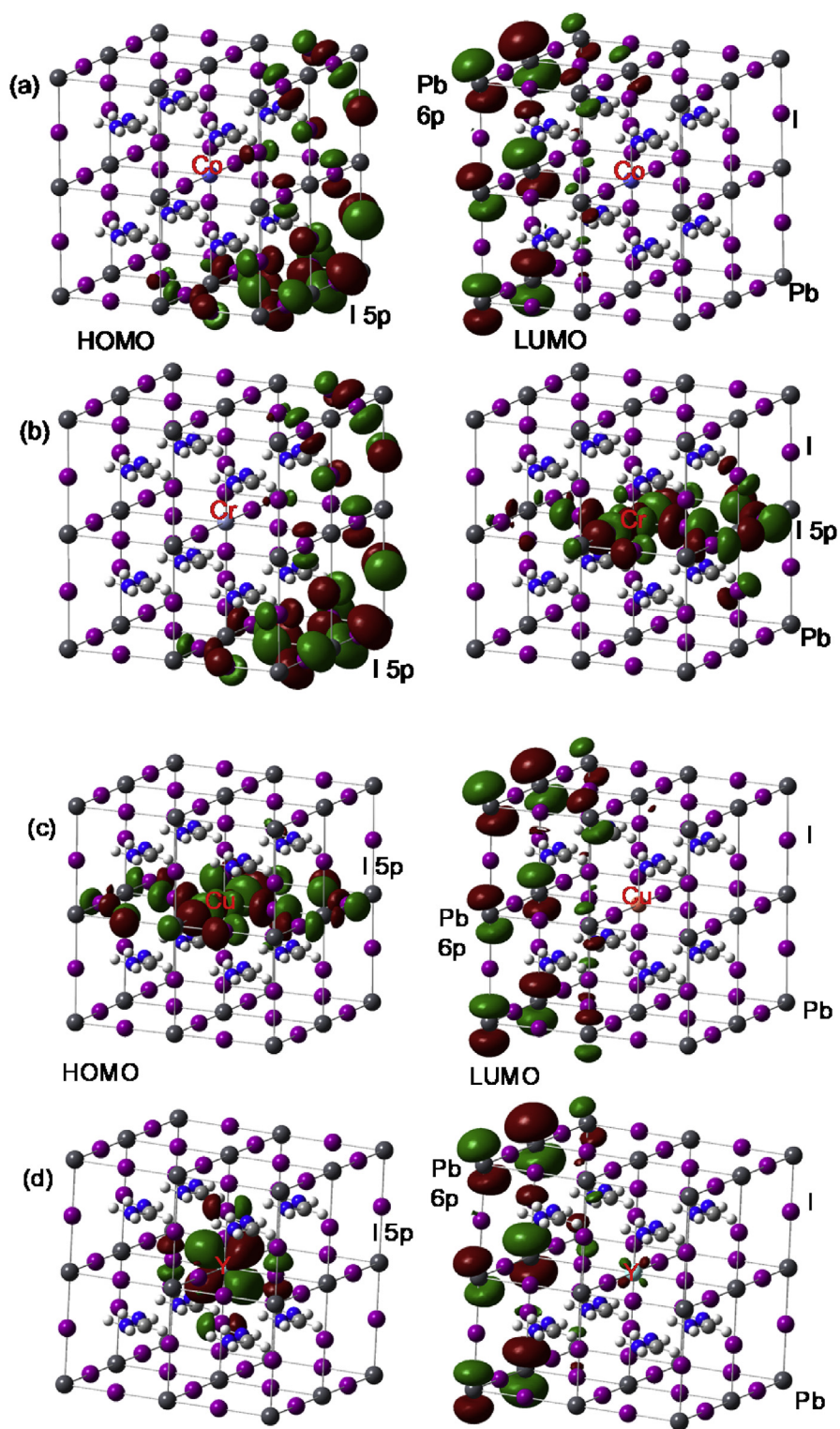
Fig. 1. Electronic structure at HOMO and LUMO of the metal (M)-incorporated FAPbI$_3$ perovskite crystals. M: (a) Co^{2+}, (b) Cr^{2+}, (c) Cu^{2+} and (d) Y^{3+}.

Co²⁺ doped FAPbI₃

Cr²⁺ doped FAPbI₃

Cu²⁺ doped FAPbI₃

Y³⁺ doped FAPbI₃

-2.7×10⁻² eV   2.7×10⁻² eV

Fig. 2. Electrostatic potential of the metal (M)-incorporated FAPbI$_3$ perovskite crystals (M = Co^{2+}, Cr^{2+}, Cu^{2+} and Y^{3+}).

**Table 1.** Mulliken atomic charges and spin density distributions of the metal atoms in the perovskite crystals.

Metal	Mulliken atomic charge/e	Spin density distribution
Co	0.35	2.22
Cr	0.47	4.59
Cu	0.28	-4.45×10^{-4}
Y	0.52	0.95

The Mulliken atomic charge and spin density distribution in the metal-incorporated FAPbI$_3$ perovskite crystal are listed in Table 1. The Mulliken atomic charges of the metal (M = Co, Cr, Cu and Y) atoms in the FAPbI$_3$ perovskite crystal were estimated to be 0.35 e, 0.47 e, 0.28 e and 0.52 e, respectively. These values were considerably small as expected value. These results indicates a considerable amount of ligand-metal-charge transfer from the 5p orbital on the I atom as ligand to the 3d orbital on the Cr atom, and metal-ligand-charge transfer from the 4d orbital on the Y atom to the 5p orbital on the iodine halogen ligand in the perovskite crystal. As listed in Table 1, the spin density distributions of the metal atom in the Co, Cr, Cu and Y-incorporated FAPbI$_3$ perovskite crystals were estimated to be 2.22, 4.59, -4.45×10^{-4}, and 0.95, respectively. The spin density distribution was a little different than the expected value of 3, 4, 1 and 1, owing to a slight amount of

electrons in the central metal released to the ligand. The spin and charge density distributions in the metal were strongly related to the magnetic properties.

The total density of states (TDOSs) of the metal-incorporated FAPbI$_3$ perovskite crystals with the $2 \times 2 \times 2$ supercell structure are shown in Fig. 3(a)−(d). Comparison of TDOSs in the metal-incorporated FAPbI$_3$ perovskite crystals was investigated. In the case of the Co and Cu-incorporated FAPbI$_3$ perovskite crystals, TDOSs with the energy levels at HOMO and LUMO did not change. In the case of the Cr and Y-incorporated FAPbI$_3$ perovskite crystals, the TDOSs and energy levels at HOMO and LUMO appeared the DOS of the $3d$ and $4d$ orbitals of the transition metal near frontier orbital. The energy levels at HOMO and LUMO in the Y-incorporated FAPbI$_3$ perovskite crystal were lowered by the slight large amount of positive charges on the Y metal, compared with other case. In the case of the Cr and Y-incorporated FAPbI$_3$ perovskite crystal, the degenerated $3d$ upper (α) spin orbitals of the Cr atom and $4d$ upper (α) and lower (β) spin orbitals of Y atom were above and below the Fermi level, as shown in Fig. 4(a) and (b). The $4s$ orbitals of the Cr and Y atom were mixed with the $6p$ orbital of the Pb atom above LUMO. The band gap between the $5p$ orbital on the I atom conjugated with the upper (α) spin of the $3d$ orbital on the Cr atom, upper spin of the $4d$ orbital on the Y atom and the $6p$ orbital of the Pb atom was narrowed. The narrowed band gap corresponds to a broad
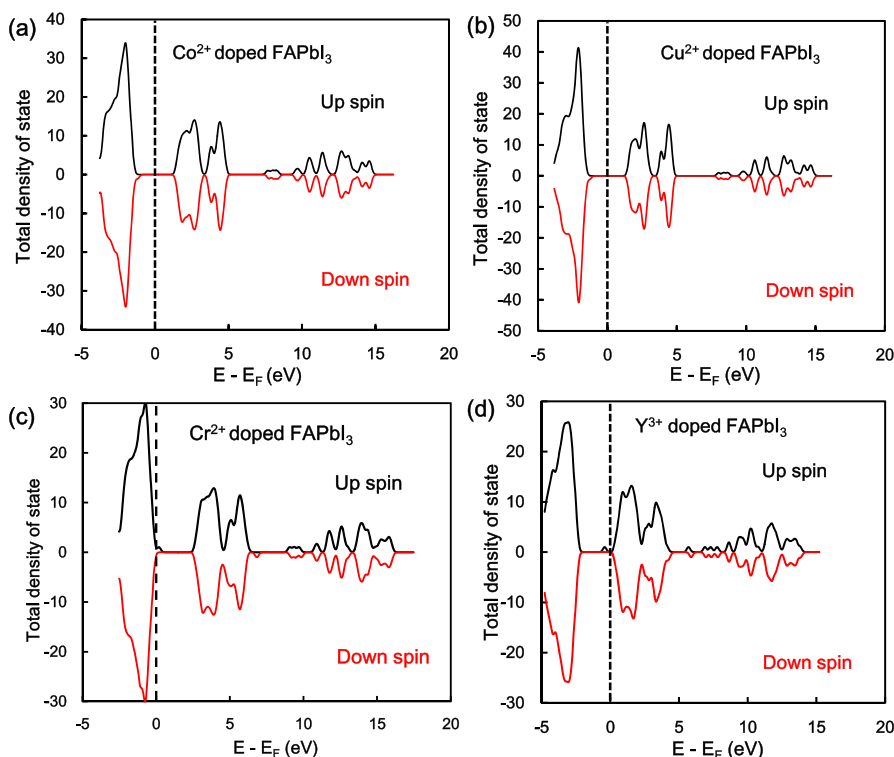
Fig. 3. Total density of states of the metal (M)-incorporated FAPbI$_3$ perovskite crystals. M: (a) Co^{2+}, (b) Cu^{2+}, (c) Cr^{2+} and (d) Y^{3+}.
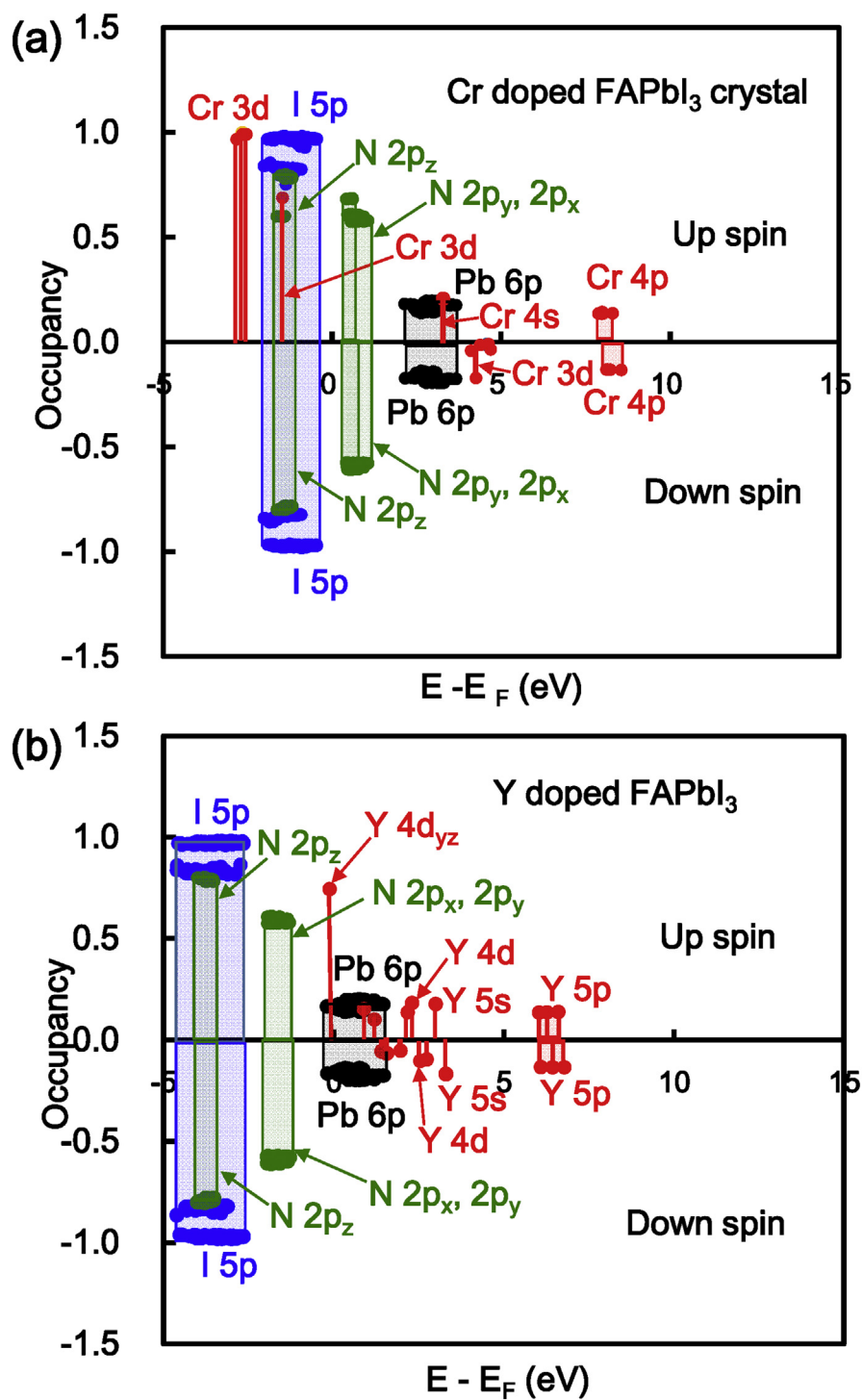
Fig. 4. Occupancy and energy levels of *s, p* and *d* orbitals of I, N, Pb and the transition metal atom near frontier orbital in (a) the Cr-incorporated FAPbI$_3$ crystal and (b) the Y-incorporated FAPbI$_3$ crystals.

absorption in the near-infrared region. The total density of state with the narrowed band gap near the frontier orbital was similar to the Mn-incorporated perovskite crystal [34, 35]. The occupancies and energy levels of the $6s$ and $6p$ orbitals of the Pb atom, the $3d$, $4s$, and $4p$ orbitals of the transition atom, and the $5p$ orbital of the I atom, and crystal splitting $3d$ orbitals near frontier orbital in the transition metal-incorporated $FAPbI_3$ perovskite crystal were reported [34, 35]. In the case of the transition metal-incorporated $FAPbI_3$ perovskite crystals, there was a six fold full occupancy on the degenerated upper spin of the $3d$ orbital on the transition metal. The occupancies, the partial density of state (PDOS), energy levels and crystal splitting provide significant information with the electron correlation based on the extent of intermixing of hybrid orbitals near the frontier orbital.

The partial density of state (PDOS) including the occupancies, energy levels of s, p and d orbitals of I, N, Pb, Cr and Y atom near frontier orbital in the Cr-incorporated perovskite crystal and the Y-incorporated perovskite crystal are shown in Fig. 4(a) and (b). In the former case using the Cr-incorporated perovskite crystal, the electron correlation was improved by crystal splitting with intermixing of hybrid orbitals between $5p$ orbital on I atom and $3d$ orbital on the Cr atom in the coordination structure. For other case, TDOS and PDOS around the Fermi level of the $3d$ orbital on the Cr atom in the Half-Heusler Alloys XCrZ was discussed [36]. In the latter case using the Y-incorporated perovskite crystal, promotion of charge transfer from isolated $4d$-orbital in Y atom to itinerant $6p$-orbital in Pb atom improved the carrier generation, diffusion length, electron mobility and the photovoltaic performance.

The electronic structures of the metal-incorporated $FAPbI_3$ perovskite crystals are related to the electronic correlation, which influences the carrier generation and diffusion, and the photovoltaic performance. These materials will be applied to the photo-induced magnetic devices with a wide range absorption in the near-infrared region. In the standard case using the $FAPbI_3$ perovskite crystal, there was partial occupancy of the $6p$ orbital of the Pb atom, and full occupancy of the $5p$ orbital of the I atom near the frontier orbital. The occupied $5p$ orbital of the I atom was near HOMO, and the partially occupied $6p$ orbital of the Pb atom was near LUMO. The electronic structure with the band gap of the HOMO-LUMO levels is associated with the photo-generation and diffusion, carrier mobility, photovoltaic and optical properties. The photovoltaic and optical properties of the metal-incorporated $FAPbI_3$ perovskite crystal depend on the electron structure, carrier generation and charge-transfer with electronic correlation between the itinerant carriers on $5p$ orbital of the halogen atom, the $6p$ orbital of the Pb atom, and the localized spin on $3d$ orbital of the transition metal. The electronic correlation are decided on the extent of inmixing of hybrization between the itinerant electron and localized spin on $3d$ orbital of the transition metal near the ligand under electric field gradient. The photovoltaic and optical properties were considered on the basis of the electronic structure in a recent publication [33, 34, 35, 36, 37, 38, 39, 40].

The energy levels at HOMO and LUMO, energy band gap (E_g), valence band maximum (VBM) and conduction band minimum (CBM) are listed in Table 2. As the calculated results of the transition metal (Cu, Co, Fe, Cr, and Y) incorporated FAPbI$_3$ perovskite crystals as cluster model with the 2 × 2 × 2 supercell structure, the energy levels at HOMO and LUMO lowered in the range of −17 eV and −15 eV, yielding the narrow band gap of 0.4−1.4 eV. The relative comparison of the energy levels of the cluster model with supercell of 2 × 2 × 2 at positive charge was investigated. As the reference of the FAPbI$_3$ perovskite crystals using cluster model with supercell of 2 × 2 × 2 at positive charge of +8, the energy levels at HOMO and LUMO, and E_g were estimated to be −17.6 eV, −14.9 eV and 2.7 eV. The positive charge in the perovskite crystal lowed the energy levels at HOMO and LUMO, yielding increase of the energy gap. The band gap of E_g was overestimated. The energy levels and band gap of the cluster model was influenced by the charge and the number of cell in the perovskite crystal. In the case of the periodic structure of the FAPbI$_3$ perovskite crystals at neutral state, cell range and number of k point were designated to be 100 and 10 as condition. The energy levels at HOMO and LUMO and E_g were estimated to be −3.6 eV, −2.1 eV and 1.5 eV. The periodic structure with the cell range of 100 narrowed the band gap of E_g. The neutral state increased the energy levels at HOMO and LUMO. In the case of the periodic structure, the calculated result will explain the experimental behaviour.

Additive effect of transitional metals into the perovskite crystal was investigated. The slight incorporation of the Cr and Y metals into the perovskite crystal narrowed

**Table 2.** Energy levels at HOMO and LUMO, and energy band gap (E_g) of the perovskite crystals.

Cal. (UB3LYP, Cell 8)	HOMO (eV)	LUMO (eV)	E_g (eV)	Ref.
Cu:FAPbI$_3$	−16.8	−15.5	1.4	This work
Co:FAPbI$_3$	−16.9	−15.6	1.3	This work
Fe:FAPbI$_3$	−17.6	−16.6	1.1	This work
Cr:FAPbI$_3$	−17.7	−17.3	0.4	This work
Y:FAPbI$_3$	−15.6	−14.8	0.8	This work
FAPbI$_3$	−17.6	−14.9	2.7	[34]
	VBM (eV)	CBM (eV	E_g (eV)	Ref.
MA (63Pb:1Co)I$_3$ (Exp.)	−6.2	−4.6	1.6	[30]
MA$_2$CuCl$_4$ (Exp.)			2.1	[38]
CuBr$_2$-added MAPbI$_3$ (Exp.)			1.6	[39]
FAPbI$_3$ (Exp.)	−5.4	−3.9	1.5	[1]
FAPbI$_3$ (PBEPBE, Cell 100)	−3.6	−2.1	1.5	This work

VBM: valence band maximum, CBM: conduction band minimum.

the band gap, corresponding to the optical absorption near the visible-near-infrared region. The experimental band gaps of the perovskite crystal with complete replacement of lead atom was large, as compared with the band gap of the $FAPbI_3$ perovskite crystals. In the case of real crystal doped with the metal, the experimental energy levels at VBM and CBM, and E_g in the hybrid Pb/Co or Cu based perovskite crystals were increased as listed in Table 2 [30, 38, 39]. The behaviour of energy levels at VBM and CBM, and E_g indicates electron-donating and *p*-type semiconductor. There is a need for experimental and theoretical consideration of the electron correlation between the itinerant electron and localized $3d$ orbital in the transition metal.

The total and partial density of state, occupancies and energy levels changed near the frontier orbital, as shown in Figs. 3 and 4. The slight incorporation of the metal into the perovskite crystal generated the $3d$ orbital near the frontier orbital with narrowing band gap, as shown in Figs. 3(c), (d) and 4. The metal-ligand charge transfer (MLCT) and ligand-metal charge transfer (LMCT) will promote the photo-induced carrier generation to improve the carrier mobility and photovoltaic performance. The partial DOS and crystal splitting of the $3d$-orbital on the metal in the crystal will be investigated by experimental results using NMR, electron paramagnetic resonance, photoemission spectroscopy, X-ray photoelectron spectroscopy and quantum calculation.

The calculated optical absorption spectra and oscillation strength of the Cr, Fe and Y-incorporated $FAPbI_3$ perovskite crystals as cluster model with the $2 \times 2 \times 2$ supercell structure are shown in Fig. 5(a) and (b). As shown in Fig. 5(a), the optical spectra of the Y, Fe and Cr-incorporated $FAPbI_3$ perovskite crystals were broadened in a wide range of 2,000−20,000 nm, which was in the infrared region. In the case of the Y-incorporated $FAPbI_3$ perovskite crystal as shown in Fig. 5(b), first excited
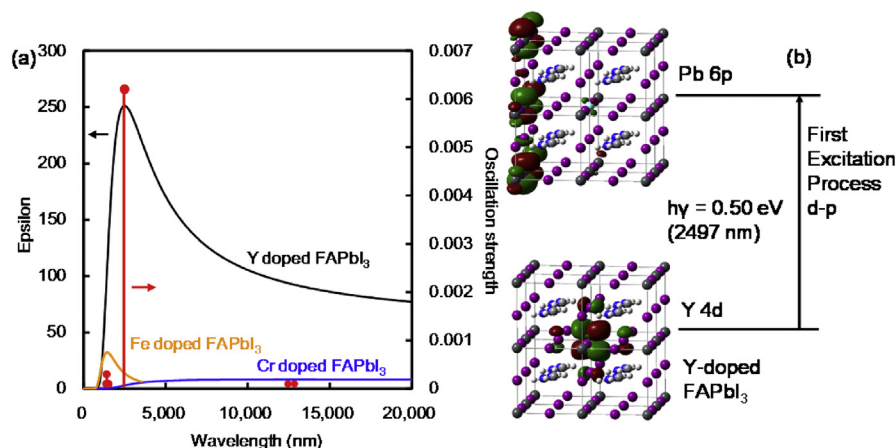
Fig. 5. (a) Optical absorption spectra and (b) first excitation process of the metal-incorporated $FAPbI_3$ perovskite crystals calculated by TD-DFT.

process was based on the energy transition process from the ground levels of the $4d$ orbital on the Y atom to the excited levels on the $6p$ orbital of the Pb atom in the crystal. In the case of the Cr-incorporated $FAPbI_3$ perovskite crystal, the first excited process was based on the transition process between the ground levels on the $5p$ orbital of the iodine halogen ligand and the excited levels of the $3d$ orbital on the metal. The LMCT contributed to a broad-band optical absorption spectrum near infrared region. Especially, the photovoltaic and optical properties will be explained by electronic transition based on LMCT and d-d transition on the Y, Cr and Fe metals with Jahn−Teller distortion in the octahedral coordination structure in the perovskite crystal [28, 30, 34, 35, 36, 37]. Based on the experimental results of the photovoltaic and optical properties, the Cu-based perovskite crystal with the distorted coordination structure had narrow band gap between d-d transitions, corresponding to a broad absorption in the near-infrared region [34, 35, 36]. Control of coordination structure with the electronic correlation in the perovskite crystal is important to improve the photovoltaic and optical properties with a wide-range of optical spectra in the ultraviolet-visible-near-infrared region.

The calculated Raman and IR spectra of the perovskite crystal are shown in Fig. 6(a)−(d). As shown in Fig. 6(a) and (b), the strong intensity of vibration modes in Raman spectra of 100, 140, 300, 680, 750, 890, 1530, 3290, 3350, 3670 and 4430
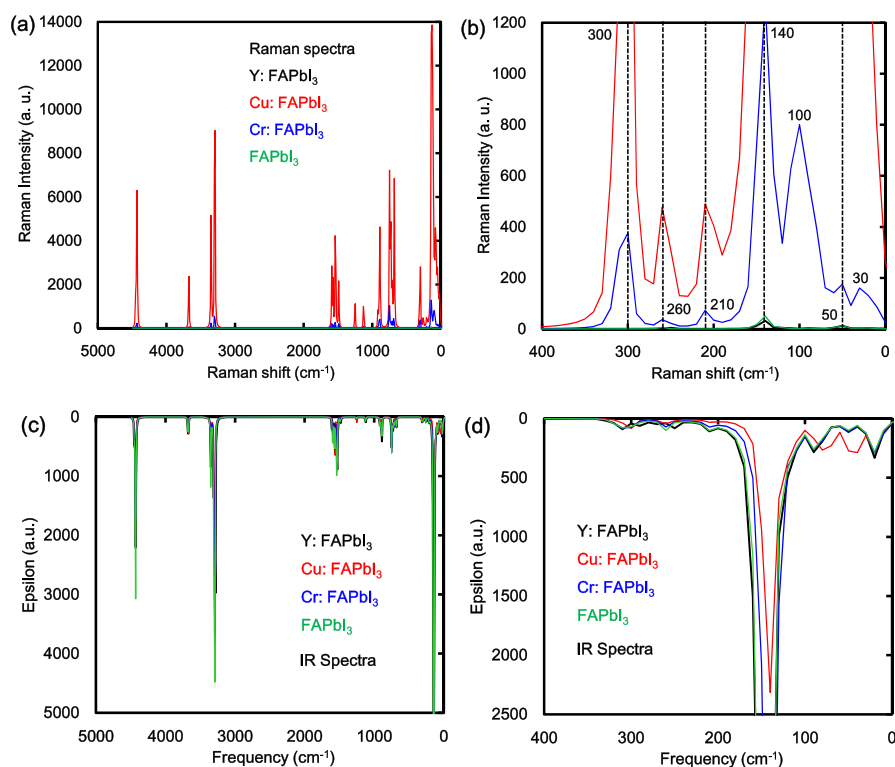
Fig. 6. Calculated (a), (b) Raman and (c), (d) IR spectra of the perovskite crystal in the normal and enlarged view of frequency.

cm^{-1} were assigned to the bending and stretching mode of FA in the Cu and Cr incorporated $FAPbI_3$ perovskite crystal. As shown in Fig. 6(b), the medium intensity of vibration modes in Raman of 30, 100 and 140 cm^{-1} were identified with asymmetric stretching mode between Cr, Cu and I atoms as ligand in the coordination cubic structure. The intensities on the vibration modes in the Cu and Cr incorporated $FAPbI_3$ perovskite crystal were strongly increased, as compared with those of Y incorporated $FAPbI_3$ crystal and standard reference using the $FAPbI_3$ perovskite crystal. As shown in Fig. 6(c) and (d), the vibration modes in IR spectra of 23, 100, 133, 140, 300, 678, 732, 746, 752, 882, 1252, 1533, 1570, 1573, 1590, 3290, 3298, 3300, 3345, 3393 and 4430 cm^{-1} were assigned to the bending mode of N-C and N-H bonds of FA in the perovskite crystal. The strong intensity of vibration modes in IR spectra of 142 and 150 cm^{-1} were identified with stretching mode between Pb and I atom as ligand in the coordination structure. The vibration modes in IR spectra of 5, 42 and 141 cm^{-1} were based on stretching mode between Cu and I atom as ligand in the coordination structure. The calculated vibration modes in Raman and IR spectra were similar to the experimental results [12, 14, 41]. The vibration behavior of the Raman and IR spectra were associated with change of polarization and distortion of the coordination structure near the ligand field. The electron-lattice interaction as phonon effect in the transition metal incorporated perovskite crystal will influence the photovoltaic properties based on the carrier diffusion.

The calculated chemical shifts of I-NMR and Pb-NMR in the metal-incorporated $FAPbI_3$ crystals are shown in Fig. 7. The effect of the incorporation of metal atoms such as Cr, Cu, Co, Fe and Y atoms in the $FAPbI_3$ perovskite crystals on the chemical shift of I-NMR and Pb-NMR was investigated. The chemical shifts of I-NMR in the Cr, Fe and Y-incorporated $FAPbI_3$ perovskite crystals were slightly split, and the degeneracy was increased by the symmetry crystal field effect. In the case of the Co and Cu-incorporated $FAPbI_3$ crystals, the chemical shifts of I-NMR were markedly
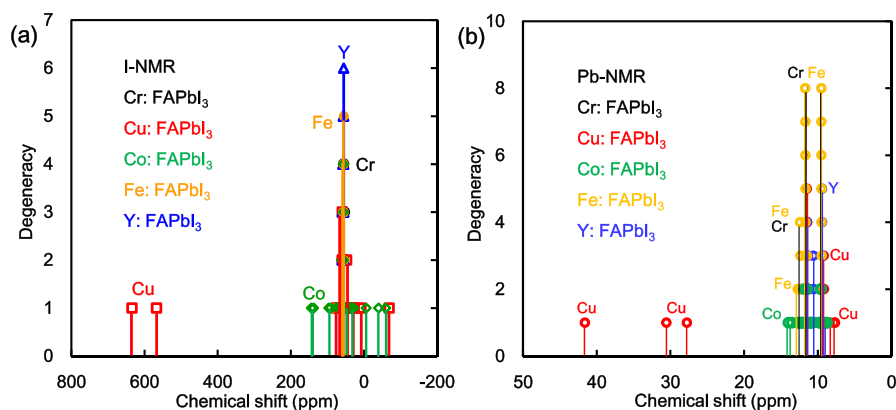
Fig. 7. The calculated chemical shifts of (a) I-NMR and (b) Pb-NMR in the metal-incorporated $FAPbI_3$ perovskite crystals.

split in a wide range from −70 ppm to 640 ppm. The chemical shifts of I-NMR near 600 ppm and 180 ppm were based on the magnetic interaction near the nearest iodine ligand conjugated with the atom in the perovskite crystal. Similarly, the chemical shifts of Pb-NMR in the Cr, Fe and Y-incorporated $FAPbI_3$ crystals were slightly split by the symmetry effect. The chemical shifts of Pb-NMR in the Co and Cu-incorporated $FAPbI_3$ crystals were widely split in the range of 8 ppm−42 ppm. The chemical shifts of Pb-NMR near 30 ppm and 40 ppm were based on the magnetic interaction near the ligand field in the perovskite crystal. The magnetic behaviour were originated in the nearest-neighbour nuclear magnetic interaction of the nuclear quadrupole interaction based on electronic field graduate (EFG) with asymmetry parameter (η) of the Co and Cu metals and I atom with multi-nuclear spins of 7/2, 3/2 and 5/2 [33]. The magnetic behaviour of the chemical shift of Pb-NMR and I-NMR was directly related by the symmetry effect of the coordination structure near the ligand field in the perovskite crystal. The chemical shifts of I-NMR and Pb-NMR in the perovskite crystals will depend on the electronic structure near frontier orbital in the perovskite crystal with the crystal phase including cubic, tetragonal and orthorhombic phases. As the calculation model based on the experimental results, the crystal structure was assumed to be a cubic crystal system. The magnetic properties depended on the perturbation of coordination structure with the nearest-neighbour magnetic interaction based on the charge distribution in the perovskite crystals. The magnetic properties were reflected by extent of the electron correlation based on the magnetic interaction.

The allowed NMR transitions can be explained by the energy level diagram of the transition atoms in the perovskite crystal. The energy levels of the transition metal in the perovskite crystal depend on the coordination structure near the ligand field. The degeneracy of the multiplet splits into each ground state in the magnetic field. The multi-separated transition is based on the hyperfine coupling between the electrons spin and nuclear spins in the multi-nuclear transition metal and the iodine halogen ligands. The separated states are considerably shifted by the nuclear quadrupole interaction with slight perturbation of the coordination structure near the ligand field of the transition metal. The nuclear quadrupole interaction is related to the nuclear quadrupole moment based on the V-tensor of electric field gradient (EFG), and asymmetry parameter (η), generated by charge distribution around the nucleus. In the case of the Cu and Co atom incorporated perovskite crystal as shown in Fig. 7(a) and (b), the chemical shifts of I-NMR and Pb-NMR were markedly split and shifted by nearest-neighbour nuclear quadrupole interaction in proportion to the extent of the V-tensor of EFG and η with a lack of balance in the charge density distribution. The perturbation of the coordination structure near the ligand field was associated with the electron correlation with inmixing of the hybrization between $3d$ and $4d$ orbital in the metal and $5p$ orbital of halogen atom in the perovskite crystal. The slight perturbation of the coordination structure was confirmed by splitting

of chemical shift and the vibration modes of the Cu and Cr atom incorporated perovskite crystals, as shown in calculated NMR, Raman and IR spectra. Accordingly, controlling of the coordination structure near the ligand field as Jahn-Teller effect and the electron correlation based on the magnetic interaction is important factors to optimize with tuning the carrier mobility, the photovoltaic and optical properties with a broad absorption near the UV-*vis*-near-infrared region. The photovoltaic and optical properties are associated with the electronic correlation based on the charge transfer process between the transition metal and halogen atom, metal ligand charge transfer (MLCT) in the perovskite crystal. The electronic correlation and perturbation of the coordination structure with electron lattice interaction as phonon effect is important factor to control the photovoltaic performance, which expect a high potential of the photovoltaic devices.

4. Conclusion

Perovskite based solar cells using transition metal incorporated $FAPbI_3$ perovskite compounds varied with molar ratio of transition metal and halogen anion have high potential to control the photovoltaic, optical and magnetic properties. The incorporation and substitution of the transition metals in the perovskite crystal influenced the electronic structure, optical and magnetic properties. The slight perturbation of coordination structure in the metal-incorporated $FAPbI_3$ perovskite crystals as the isolated dilution system is important factor to make design of the photovoltaic solar cells and photo-induced magnetic devices. The effects of slight incorporation of the metals such as Cr, Co, Cu and Y atoms into the perovskite crystal on the electronic structures, chemical shifts and optical absorption spectra were investigated by the first-principle calculation using density functional theory. In the case of the Cr^{2+}, Cu^{2+} and Y^{3+}-incorporated $FAPbI_3$ perovskite crystal, the electron density distribution of *d-p* hybrid orbital on the transition metal and iodine halogen ligand were delocalized at the frontier orbital. The total and partial density of state appeared the $3d$-*p* hybrid orbital near frontier orbital, yielding the narrowing band gap as well as the wide broad absorption in the visible-near-infrared region. The optical and magnetic properties were originated in the coordination structure and the electronic correlation between the transition metal, the Pb and I atoms in the perovskite crystal. The vibration modes of the Raman and IR spectra were associated with change of polarization and slight distortion of the coordination structure in the perovskite crystal. The transport and photovoltaic properties were influenced by the electronic correlation with electron lattice interaction as phonon effect. Considerable splitting of the chemical shift of I-NMR and Pb-NMR was caused by crystal field splitting as Jahn-Teller effect and nearest-neighbor nuclear quadrupole interaction based on the charge distribution. The slight perturbation of the coordination structure caused by the insertion of transition metal affected the photo-induced carrier generation and diffusion,

mobility, and the photovoltaic and optical properties. Control of the coordination structure, the electronic correlation and the magnetic interactions based on the charge distribution in the perovskite crystal is important factor to optimize with tuning the photovoltaic and optical properties with the wide broad absorption in the UV-*vis*-near-infrared region.

Declarations

Author contribution statement

Atsushi Suzuki: Conceived and designed the analysis; Analyzed and interpreted the data; Contributed analysis tools or data; Wrote the paper.

Takeo Oku: Contributed analysis tools or data; Wrote the paper.

Funding statement

Competing interest statement

The authors declare no conflict of interest.

Additional information

No additional information is available for this paper.

References

[1] A.A. Zhumekenov, M.I. Saidaminov, M.A. Haque, E. Alarousu, S.P. Sarmah, B. Murali, I. Dursun, X.H. Miao, A.L. Abdelhady, T. Wu, O.F. Mohammed, O.M. Bakr, Formamidinium lead halide perovskite crystals with unprecedented long carrier dynamics and diffusion length, ACS Energy Lett. 1 (1) (2016) 32−37.

[2] Y. Umemoto, A. Suzuki, T. Oku, Effects of halogen doping on the photovoltaic properties of $HC(NH_2)_2PbI_3$ perovskite solar cells, AIP Conf. Proc. 1807 (2017), 020011-1-10.

[3] M. Saliba, T. Matsu, J.Y. Seo, K. Domanski, J.P.C. Baena, M.K. Nazeeruddin, S.M. Zakeeruddin, W. Tress, A. Abate, A. Hagfeldt, M. Grätzel, Cesium-containing triple cation perovskite solar cells: improved stability, reproducibility and high efficiency, Energy Environ. Sci. 9 (2016) 1989−1997.

[4] A.D. Jodlowski, C.R. Carmona, G. Grancini, M. Salado, M. Ralaiarisoa, S. Ahmad, N. Koch, L. Camacho, G. Miguel, M.K. Nazeeruddin, Large guanidinium cation mixed with methylammonium in lead iodide perovskites for 19% efficient solar cells, Nat. Energy 2 (2017) 972−979.

[5] H.X. Zhu, J.M. Li, Electronic structure of organometal halide perovskite $CH_3NH_3BiI_3$ and optical absorption extending to infrared region, Sci. Rep. 6 (2016), 37425-1-9.

[6] K. Suzuki, A. Suzuki, M. Zushi, T. Oku, Microstructures and properties of $CH_3NH_3PbI_{3-x}Cl_x CH_3NH_3PbI_{3-x}Cl_x$ hybrid solar cells, AIP Conf. Proc. 1649 (2015) 96−101.

[7] A. Suzuki, H. Okada, T. Oku, Fabrication and characterization of $CH_3NH_3PbI_{3-x-y}Br_xCl_y$ perovskite solar cells, Energies 9 (5) (2016), 376-1-11.

[8] C.C. Stoumpos, C.M.M. Soe, H. Tsai, W. Nie, J.C. Blancon, D.H. Cao, F. Liu, B. Traoré, C. Katan, J. Even, A.D. Mohite, M.G. Kanatzidis, High members of the 2D ruddlesden-popper halide perovskites: synthesis, optical properties, and solar cells of $(CH_3(CH_2)_3NH_3)_2(CH_3NH_3)_4Pb_5I_{16}$, Chem 2 (3) (2017) 427−440.

[9] A. Amat, E. Mosconi, E. Ronca, C. Quarti, P. Umari, M.K. Nazeeruddin, M. Grätzel, F.D. Angelis, Cation-induced band-gap tuning in organohalide perovskites: interplay of spin−orbit coupling and octahedra tilting, Nano Lett. 14 (6) (2014) 3608−3616.

[10] H.J. Feng, T.R. Paudel, E.Y. Tsymbal, X.C. Zeng, Tunable optical properties and charge separation in $CH_3NH_3Sn_xPb_{1-x}I_3/TiO_2$-based planar perovskites cells, J. Am. Chem. Soc. 137 (25) (2015) 8227−8236.

[11] G. Giorgi, J. Fujisawa, H. Segawa, K. Yamashita, Organic-inorganic hybrid lead iodide perovskite featuring zero dipole moment guanidinium cations: a theoretical analysis, J. Phys. Chem. C 119 (2015) 4694−4701.

[12] B.W. Park, S.M. Jain, X. Zhang, A. Hagfeldt, G. Boschloo, T. Edvinsson, Resonance Raman and excitation energy dependent charge transfer mechanism in halide-substituted hybrid perovskite solar cells, ACS Nano 9 (2) (2015) 2088−2101.

[13] H.J. Feng, W. Deng, K. Yang, J. Huang, X.C. Zeng, Double perovskite Cs_2BBiX_6 (B = Ag, Cu; X = Br, Cl)/TiO_2 heterojunction: an efficient Pb-free perovskite interface for charge extraction, J. Phys. Chem. C 121 (8) (2017) 4471−4480.

[14] F. Brivio, J.M. Frost, J.M. Skelton, A.J. Jackson, O.J. Weber, M.T. Weller, A.R. Goni, A.M.A. Leguy, P.R.F. Barnes, A. Walsh, Lattice dynamics and vibrational spectra of the orthorhombic, tetragonal, and cubic phases of methylammonium lead iodide, Phys. Rev. B 92 (2015), 144308-1-8.

[15] P. Umari, E. Mosconi, F.D. Angelis, Relativistic GW calculations on $CH_3NH_3PbI_3$ and $CH_3NH_3SnI_3$ perovskites for solar cell applications, Sci. Rep. 4 (2014), 4467-1-7.

[16] Y. Wang, T. Gould, J.F. Dobson, H. Zhang, H. Yang, X. Yao, H. Zhao, Density functional theory analysis of structural and electronic properties of orthorhombic perovskite $CH_3NH_3PbI_3$, Phys. Chem. Chem. Phys. 16 (2014) 1424−1429.

[17] C. Roiland, G.T. Allard, K. Jemli, B. Alonso, J.C. Ameline, R. Gautier, T. Bataille, L.L. Pollès, E. Deleporte, J. Even, C. Katan, Multinuclear NMR as a tool for studying local order and dynamics in $CH_3NH_3PbX_3$ (X = Cl, Br, I) hybrid perovskites, Phys. Chem. Chem. Phys. 18 (2016) 27133−27142.

[18] A. Senocrate, I. Moudrakovski, G.Y. Kim, T.Y. Yang, G. Gregori, M. Grätzel, J. Maier, The nature of ion conduction in methylammonium lead iodide: a multimethod approach, Angew. Chem. 56 (27) (2017) 7755−7759.

[19] D.J. Kubicki, D. Prochowicz, A. Hofstetter, P. Péchy, S.M. Zakeeruddin, M. Grätzel, L. Emsley, Cation dynamics in mixed-cation $(MA)_x(FA)_{1−x}PbI_3$ hybrid perovskites from solid-state NMR, J. Am. Chem. Soc. 139 (29) (2017) 10055−10061.

[20] D.J. Kubick, D. Prochowicz, A. Hofstetter, S.M. Zakeeruddin, M. Grätzel, L. Emsley, Phase segregation in Cs-, Rb- and K-doped mixed-cation $(MA)_x(FA)_{1−x}PbI_3$ hybrid perovskites from solid-state NMR, J. Am. Chem. Soc. 139 (40) (2017) 14173−14180.

[21] B. Náfrádi, P. Szirmai, M. Spina, H. Lee, O.V. Yazyev, A. Arakcheeva, D. Chernyshov, M. Givert, L. Forró, E. Horváth, Optically switched magnetism in photovoltaic perovskite $CH_3NH_3(Mn:Pb)I_3$, Nat. Commun. 7 (2016), 13406-1-8.

[22] W.J. Mir, M. Jagadeeswararao, S. Das, A. Nag, Colloidal Mn-doped cesium lead halide perovskite nanoplatelets, ACS Energy Lett. 2 (3) (2017) 537−543.

[23] A. Biswas, R. Bakthavatsalam, J. Kundu, Efficient exciton to dopant energy transfer in Mn^{2+}-doped $(C_4H_9NH_3)_2PbBr_4$ two-dimensional (2D) layered perovskites, Chem. Mater. 29 (18) (2017) 7816−7825.

[24] S. Berri, D. Maouche, M. Ibrir, B. Bakri, Electronic structure and magnetic properties of the perovskite cerium manganese oxide from ab initio calculations, Mater. Sci. Semicond. Process. 26 (2014) 199−204.

[25] M.D. Sampson, J.S. Park, R.D. Schaller, M.K.Y. Chan, A.B.F. Martinson, Transition metal-substituted lead halide perovskite absorbers, J. Mater. Chem. A 5 (2017) 3578−3588.

[26] X. Li, X. Zhong, Y. Hu, B. Li, Y. Sheng, Y. Zhang, C. Weng, M. Feng, H. Han, J. Wang, Organic-inorganic copper(II)-based material: a low-toxic, highly stable light absorber for photovoltaic application, J. Phys. Chem. Lett. 8 (8) (2017) 1804−1809.

[27] S.F. Hoefler, G. Trimmel, T. Rath, Progress on lead-free metal halide perovskites for photovoltaic applications: a review, Monatsh. Chem. 148 (2017) 795−826.

[28] D. Cortecchia, H.A. Dewi, J. Yin, A. Bruno, S. Chen, T. Baikie, P.P. Boix, M. Grätzel, S. Mhaisalkar, C. Soci, N. Mathews, Lead-free $MA_2CuCl_xBr_{4-x}$ hybrid perovskites, Inorg. Chem. 55 (3) (2016) 1044−1052.

[29] M. Daub, R. Stroh, H. Hillebrecht, Synthesis, crystal structure, and optical properties of $(CH_3NH_3)_2CoX_4$ ($X =$ Cl, Br, I, $Cl_{0.5}Br_{0.5}$, $Cl_{0.5}I_{0.5}$, $Br_{0.5}I_{0.5}$), Z. Anorg. Allg. Chem. 642 (3) (2016) 268−274.

[30] M.T. Klug, A. Osherov, A.A. Haghighirad, S.D. Stranks, P.R. Brown, S. Bai, J.T.W. Wang, X. Dang, V. Bulović, H.J. Snaith, A.M. Belcher, Tailoring metal halide perovskites through metal substitution: influence on photovoltaic and material properties, Energy Environ. Sci. 10 (2017) 236−246.

[31] M.T. Weller, O.J. Weber, J.M. Frost, A. Walsh, Cubic perovskite structure of black formamidinium lead iodide, α-$[HC(NH_2)_2]PbI_3$, at 298 K, J. Phys. Chem. Lett. 6 (16) (2015) 3209−3212.

[32] J.R. Poindexter, R.L.Z. Hoye, L. Nienhaus, R.C. Kurchin, A.E. Morishige, E.E. Looney, A. Osherov, J.P.C. Baena, B. Lai, V. Bulović, V. Stevanović, M.G. Bawendi, T. Buonassisi, High tolerance to iron contamination in lead halide perovskite solar cells, ACS Nano 11 (7) (2017) 7101−7109.

[33] Z. Xiao, Y. Yan, Progress in theoretical study of metal halide perovskite solar cell materials, Adv. Energy Mater. 7 (2017), 1701136-1-20.

[34] A. Suzuki, T. Oku, First-principles calculation study of electronic structures and magnetic properties of Mn-doped perovskite crystals for solar cell applications, Jpn. J. Appl. Phys. 57 (2018), 02CE04-1-7.

[35] M. Taguchi, A. Suzuki, H. Tanaka, T. Oku, Fabrication and characterization of perovskite solar cells added with $MnCl_2$, YCl_3 or poly(methyl methacrylate), AIP Conf. Proc. 1929 (2018), 020012-1-8.

[36] X. Wang, Z. Cheng, G. Liu, Largest magnetic moments in the half-heusler alloys XCrZ (X = Li, K, Rb, Cs; Z = S, Se, Te): a first-principles study, Materials 10 (2017) 1078.

[37] H.S. Jung, N.G. Park, Perovskite solar cells: from materials to devices, Small 11 (1) (2015) 10−25.

[38] D. Cortecchia, C. Soci, M. Cametti, A. Petrozza, J.M. Rujas, Crystal engineering of a two-dimensional lead-free perovskite with functional organic cations by second-sphere coordination, ChemPlusChem 82 (2017) 681−685.

[39] Y. Shirahata, T. Oku, Effects of copper addition on photovoltaic properties of perovskite $CH_3NH_3PbI_{3-x}Cl_x$ solar cells, Phys. Status Solidi A 214 (10) (2017), 1700268-1-6.

[40] T. Nakajima, K. Sawada, Discovery of Pb-free perovskite solar cells via high-throughput simulation on the K computer, J. Phys. Chem. Lett. 8 (2017) 4826−4831.

[41] C. Quarti, G. Grancini, E. Mosconi, P. Bruno, J.M. Ball, M.M. Lee, H.J. Snaith, A. Petrozza, F.D. Angelis, The Raman spectrum of the $CH_3NH_3PbI_3$ hybrid perovskite: interplay of theory and experiment, J. Phys. Chem. Lett. 5 (2) (2014) 279−284.